Electronic Supplementary Material (ESI) for Environmental Science: Nano.

Structural Transformation of Sulfidized Zerovalent Iron And Its Impact On Long-term Reactivity†

Marco C. Mangayayam[a*], Jeffrey Paulo H. Perez[b,c], Knud Dideriksen[d], Helen Freeman[b,e], Nicolas Bovet[f], Liane G. Benning[b,c], Dominique J. Tobler[a*]

[a]*Nano-Science Center, Department of Chemistry, University of Copenhagen, Universitetsparken 5, 2100 Copenhagen, Denmark*

[b]*GFZ German Research Centre for Geosciences, Telegrafenberg, 14473 Potsdam, Germany*

[c]*Department of Earth Sciences, Free University of Berlin, 12249 Berlin, Germany*

[d]*Geological Survey of Denmark & Greenland (GEUS), Øster Voldgade 10, 1350 Copenhagen, Denmark*

[e]*School of Chemical and Process Engineering, University of Leeds, Leeds LS2 9JT, United Kingdom*

[f]*Danish Hydrocarbon Research and Technology Centre (DHRTC), Technical University of Denmark (DTU), Kongens Lyngby, Denmark*

**Corresponding author: mc.marco@chem.ku.dk and dominique.tobler@nano.ku.dk*

Content of this supporting information

This supporting information contains additional details on methods and additional data and figures to support the interpretation made in the results and discussion section. In total, this SI includes 19 pages with 16 figures, and 8 tables.

Additional details towards methods

Text S1. Chemicals used for synthesis

$FeCl_2 \cdot 4H_2O$ (99+%, Acros Organics), $NaBH_4$ (98%, Sigma Aldrich), sodium acetate (reagent grade, Sigma-Aldrich), acetic acid (99%, reagent plus), HCl (37%, Sigma-Aldrich), Na_2S $9H_2O$ (98+%, Sigma-Aldrich)

Text S2. Synthesis of S-nZVI, $FeS_{mackinawite}$, and green rust

S-nZVI: Nano-meter sized zerovalent iron, nZVI (theoretical mass: 1 g), was made by reacting 71.6 mL of 0.25 M $FeCl_2$ with 35.8 mL of 1 M $NaBH_4$. The resulting nZVI was separated from solution with a magnet and then resuspended in 120.8 mL 0.2 M acetate buffer (acetic acid-sodium acetate

mixture) inside a 160-mL crimp capped reactor and sonicated for 10 minutes. The acetate buffer was utilized to facilitate a controlled corrosion of nZVI surfaces and to dissolve any surface Fe^{2+}. Thereafter, 4.2 mL 1 M Na_2S (theoretical S/Fe: 0.23) were rapidly injected into the reactor and mixed for an additional 3 h on an orbital shaker (200 rpm). Afterwards, the particles were washed thrice with 96% degassed ethanol and then directly used in aging experiments. For initial material characterization, the washed S-nZVI were dried in a desiccator under vacuum for 48 h.

Mackinawite and green rust reference samples: Mackinawite and green rust were synthesized according to methods used in our previous study.[1,2] For mackinawite, 100 mL 50 mM Na_2S solution was titrated into 100 mL 50 mM $FeCl_2$ solution. The precipitates were washed thrice with degassed Milli-Q by centrifugation-resuspension method. For green rust, 100 mL 50 mM $FeCl_2$ solution was slowly oxidized by aeration while maintaining a pH of 7 using 1 M NaOH using a titration system. After 6.5 mL of NaOH was added, oxidation was stopped and the precipitates were isolated by vacuum filtration. These samples were dried inside a desiccator under vacuum for 48 h at room temperature and kept inside the anaerobic glovebox until use.

Table S1. Composition of artificial groundwater used in aging experiments (with and without TCE re-spiking) was based on Smith et al.[2] Dissolved oxygen was removed by sparging with N_2 for approximately 2 h prior to overnight equilibration in the anaerobic chamber.

Cations	mM	Anions	mM
K^+	0.06	CO_3^{2-}	0.83
Ca^{2+}	1.09	HCO_3^-	0.37
Na^+	0.42	NO_3^-	0.01
Mg^{2+}	0.21	$H_2PO_4^-$	0.02
		SO_4^{2-}	0.25
		Cl^-	0.51

Text S3. Details on sample preparation, handling and analyses during XRD, TEM, XPS measurements.

XRD and PDF: Approximately 50 mg of dried, solid samples were filled into borosilicate glass capillaries with an outer diameter of 0.9 mm. The capillaries were sealed with paraffin wax to avoid any air exposure during sample transport to the synchrotron facility. The used sample-to-detector (40 x 40 amorphous Si detector) distances were 18 cm and 100 cm to obtain PDF and XRD data, respectively. PDF data treatment is outlined in our previous study.[1]

PDF peak fitting to approximate phase abundance: Absolute peak intensities in PDF depend on the electron density of the atom pairs, their coordination number, the size of coherent scattering domains, the instrumental dampening, and the phase abundance. Hence, changes in peak intensities can be used to approximate the changes in phase abundance with time. We used this here to evaluate the time-dependent oxidation (i.e., depletion) of the Fe core with aging time. To do so, we fitted the PDF pattern ranging from 0.5-3.5 Å with 4 Gaussian peaks representing $Fe^{II/III}$-O, Fe^{0}-Fe^{0} (1^{st} shell), Fe^{0}-Fe^{0} (2^{nd} shell) and Fe^{II}-$Fe^{II/III}$. To minimize the effects of instrumental dampening, small coherent scattering domains, and variation in electron density of the atom pairs, which influence peak heights, we used the 1^{st} shell Fe^{0}-Fe^{0} peak at 2.53 Å to represent the fraction of remaining Fe^{0} core (cubic coordination), while the peak at 3.19 Å (i.e., Fe^{II}-$Fe^{II/III}$, octahedral coordination) was used to characterize the fraction of formed corrosion product (i.e., GR_{CO3} and/or WR Table S3, Figure S4). The difference in coordination numbers were accounted for by normalizing the cubic coordination with respect to octahedral coordination (i.e., multiplying with 6/8). In the fitting, we have not considered the impact to the peak intensity caused by termination ripples from other peaks. Therefore, to verify the robustness of this approach we also calculated theoretical PDFs of Fe^{0} and green rust mixtures with different molar fractions (Table S2). The linear relationship (slope = 0.96, R^2 = 0.99) between the theoretical molar amount of Fe^{0} and the calculated amount of Fe^{0} based from Gaussian heights, supports the validity of this routine (Figure S1).

Table S2. To validate the applied PDF peak fitting procedure (Text S3), we ran a similar Gaussian fitting routine using hypothetical PDFs with known fractions of α-Fe and green rust. The crystallographic information files for α-Fe and green rusts were taken from Wyckoff et al.[3] and Chistiansen et al.[4], respectively.

Fe^0	Green rust	Peak height of Fe^{II}-O in octahedral coordination	Peak height of Fe^0-Fe^0 in cubic coordination	Peak height of Fe^0-Fe^0 in cubic coordination	Peak height of Fe^{II}-Fe^{II} in octahedral coordination	R^2 value
20%	80%	2.23	1.45	0.63	4.28	0.995
40%	60%	1.51	3.06	0.73	3.32	0.999
50%	50%	1.33	3.99	0.98	2.96	0.999
60%	40%	1.03	4.87	1.19	2.49	0.999
80%	20%	0.43	6.70	1.21	1.94	0.999

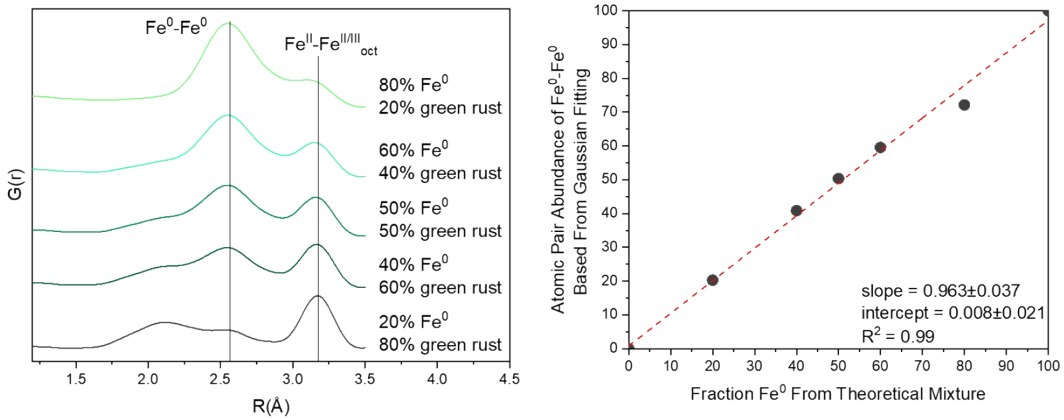

Figure S1. The calculated PDF patterns from theoretical mixtures of Fe^0 (representing the reduced phase) and green rust (representing the oxidized phase) showed that a linear relationship exists between the height of first Fe^0-Fe^0 peak and the fraction of Fe^0 in the sample mixture.

TEM and SEM: Approximately 500 µL of sample suspension were 10x diluted in degassed 96% ethanol. The resulting suspension was drop-casted onto a holey amorphous carbon-coated Cu TEM grid placed on top of vacuum filtration set-up and left to dry for ca. 15 minutes. The grid was loaded onto a TEM grid box and transported to the TEM instrument using an anaerobic jar to minimize air

exposure (< 1 minute). The TEM grids were then individually loaded into a single tilt holder and inserted to TEM instrument. Image analyses and measurements were made in Gatan Digital Micrograph and ImageJ. For SEM, 5 µL diluted sample suspension were drop casted directly to an aluminium stub and dried in the desiccator under vacuum for 2 h. The aluminium stub was transported via SEM stub holders in a customized anaerobic box to minimize air exposure (< 1 minute). The SEM stub was loaded on a sample stage and inserted in the SEM instrument.

XPS: Dry samples (~50 mg) were placed on an XPS aluminium stub inside the anaerobic chamber and a drop of ethanol was added to wet the samples. The stub was loaded onto an anaerobic sample holder to minimize air exposure during transport to the XPS instrument. The anaerobic holder was connected to the sample entry chamber and opened once the pressure was reduced to ca. 0.1 Pa. Spectral analyses were done in CasaXPS. Binding energy values of iron species were taken from Biesinger et al.[5] while values for sulfur species were taken from Mullet et al.[6]

Text S4. Additional details on TCE reduction rate analysis (following aging and during TCE re-spiking)

Experimental and control reactors (artificial groudwater and TCE only) were prepared in 160-mL serum bottles capped with Viton stoppers. During the experiments, the reactors were taken outside the anaerobic chamber and the bottles were placed upside down (to minimize volatilization) on an orbital shaker at 125 rpm. At specific time points, 1 mL aliquots were taken from the reactors using a Hamilton syringe-needle, and directly added to 9 mL degassed Milli-Q water inside a 20-ml glass vial before crimping. Per sampling time, two such samples were prepared for each reactor to verify sampling accuracy. The glass vials were analyzed using a Gerstel 1888 Autosampler and Agilent 6890 for headspace gas chromatography mass spectrometry (GC-MS). Prior to headspace extraction, the vials were equilibrated for 15 min at 50 °C. Approximately 1 µL of headspace was injected into a DB-624MS (Agilent) column, kept at 35 °C and then heated to 115 °C at a rate of 10 °C min^{-1}.[7]

TCE concentrations in experimental reactors (C) and control reactors (Co) were determined by integrating the peak area of TCE in the GC-MS chromatogram. The TCE reduction rate constants, k_{obs}, were calculated from the linear fitting of the natural logarithm of normalized concentration (C/C_o) as a function of time (Eq. 1). This way, any possible volatilization and experimental errors during sampling, are not factored in the derived rates.[1]

$$\ln\left(\frac{C}{C_o}\right) = -kt \tag{1}$$

For re-spiking experiments, once TCE concentration was below 5%, the reactor was re-opened in the glovebox to amend 110 µM of TCE. This initiated a new cycle of TCE reduction. Similarly, the k_{obs} for each cycles were calculated using Equation 1.

Additional data, figures, and tables towards results and discussion

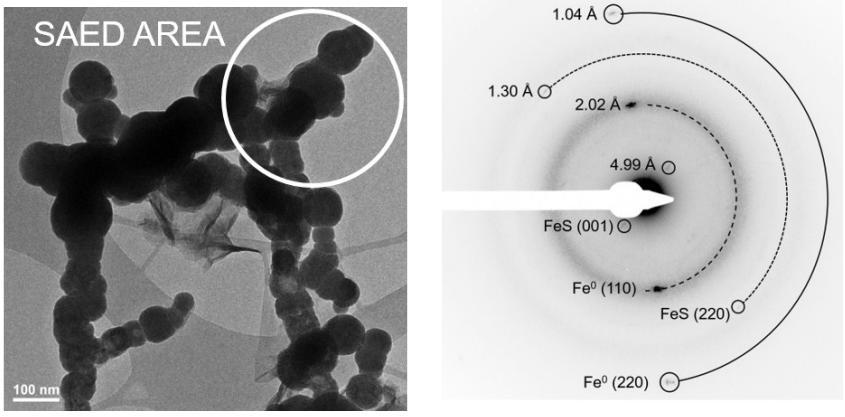

Phase assignment

d-spacing$_{meas}$	Phase	hkl	d-spacing$_{theo}$
4.99 Å	FeS_m	001	5.03 Å
2.02 Å	Fe^0	110	2.03 Å
1.30 Å	FeS_m	220	1.30 Å
1.04 Å	Fe^0	220	1.19 Å

Figure S2. Selected electron area diffraction of Figure 2a (fresh S-nZVI) showing the diffuse rings of Fe^0 and FeS.

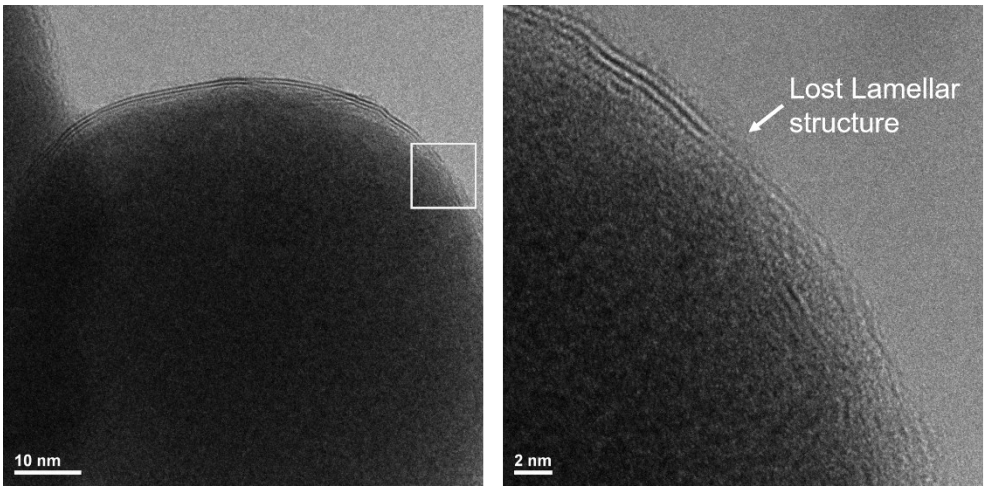

Figure S3. TEM images showing shell discontinuities in the FeS_m shell. Such defects present weak points in the shell where bulk water may be able to interact with the Fe^0 core.

Table S3. Peak height values as determined from Gaussian fitting of S-nZVI PDF distances as a function of time (details in Text S3). Estimates of phase proportions are shown in Figure S4.

Aging Time	Peak height of Fe^{II}-O in octahedral coordination (2.11Å)	Peak height of Fe^0-Fe^0 in cubic coordination (2.49Å)	Peak height of Fe^0-Fe^0 in cubic coordination (2.84Å)	Peak height of Fe^{II}-Fe^{II} in octahedral coordination (3.17Å)	R^2 value
0	1.33	8.93	3.38	0.44	0.998
5	1.49	9.09	3.63	0.50	0.994
10	1.32	8.85	3.31	0.50	0.999
20	1.50	8.05	3.17	0.89	0.998
40	2.07	5.67	2.60	2.13	0.997
60	2.62	4.58	1.83	3.25	0.997
120	2.71	3.97	1.10	3.72	0.993

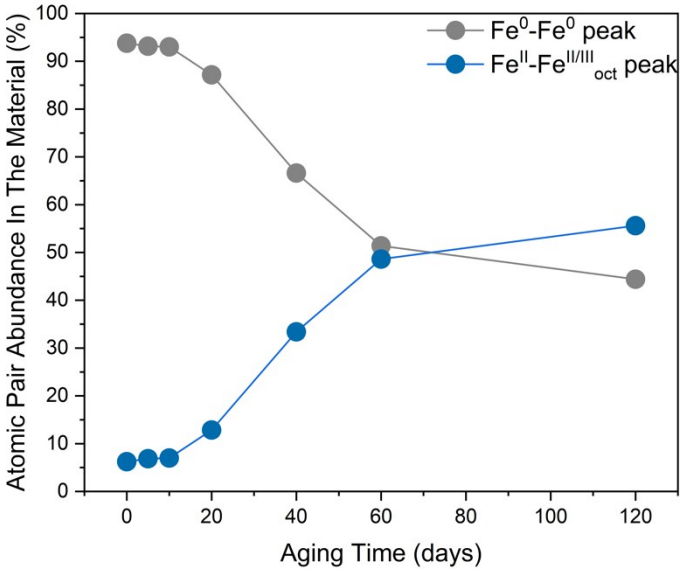

Figure S4. The data in Table S3 was plotted as a function of pair abundance within the aged S-nZVI materials. Specifically, the Fe-Fe pairs in cubic and octahedral coordination was used to represent the Fe^0 and corrosion products (i.e., GR_{CO3}, WR) respectively. Lastly, the Fe-Fe in cubic and octahedral coordination was plotted as relative percentages. This allows to visualize the rate of S-nZVI oxidation as a function of time.

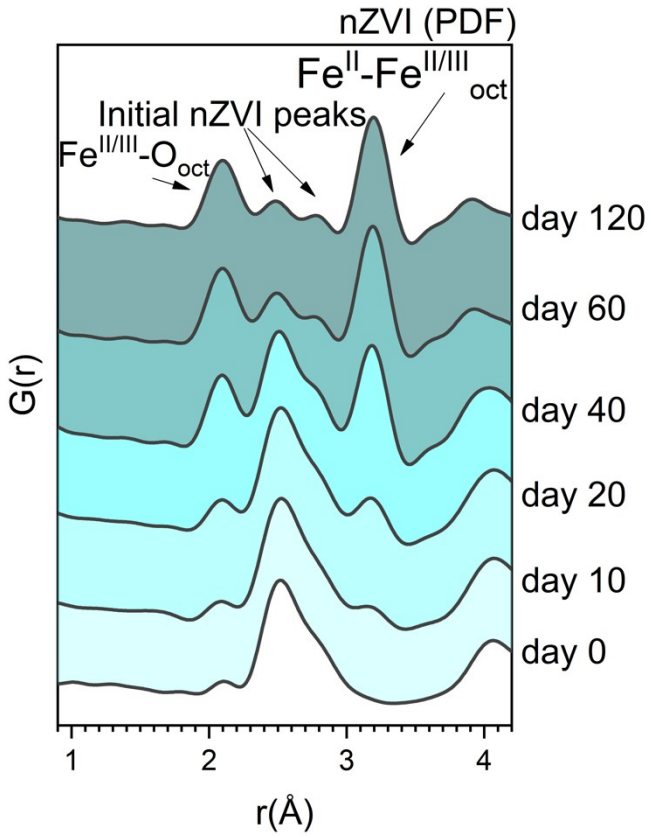

Figure S5. PDF data of non-sulfidized ZVI (nZVI) shows the appearance of Fe^{II}-O and Fe^{II}-Fe^{II} local atomic pairs, due to the formation of corrosion product during Fe^0 oxidation by water. The same PDF peak analyses as used for S-nZVI (Text S3) were applied here to approximate the rate of nZVI oxidation (i.e., corrosion product formation) as a function of aging time. Noteworthy that at 120 days nZVI aging, the intensity of first Fe^0-Fe^0 peak in cubic coordination (i.e., initial nZVI peak) may be overestimated during peak height determination due to contributions by termination ripples (visible in the PDF of the green rust reference samples), an artefact from truncation of Fourier transformation of the structure function. This could mean that for the 120-day spectra, the calculated approximate amount of nZVI may be higher than the true value. Nonetheless, the trends observed here, are still in line with our key result that nZVI electrons are depleted quickly by interaction with water (Figure S6).

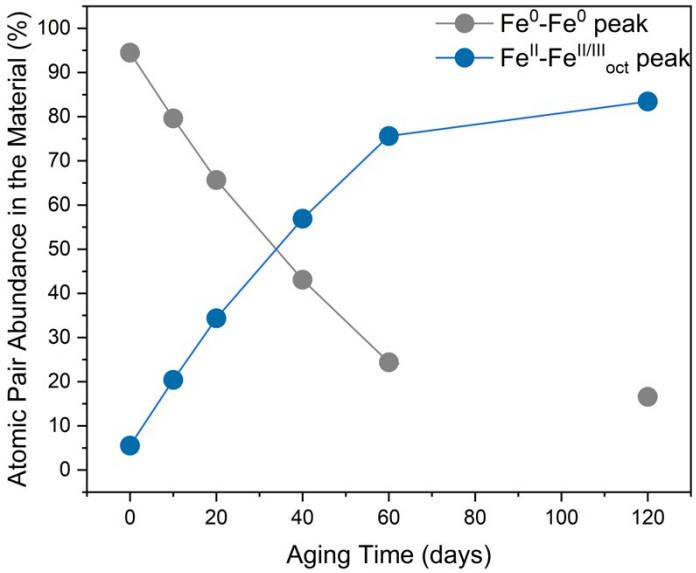

Figure S6. The atomic pair abundance in aged nZVI based on PDF peak height analyses (Text S3). This shows that Fe^0 oxidation (i.e., formation of corrosion products) occurred instantaneously upon contact with groundwater, as shown by the continuous decline in Fe^0-Fe^0 atomic pairs (i.e., nZVI material) and concomitant increase in Fe^{II}-$Fe^{II/III}$ atomic pairs. This is in contrast to S-nZVI aging, where little oxidation was observed for the first 10 days of groundwater exposure (Figure S4), underpinning the different oxidation behavior between nZVI and S-nZVI particles.

Table S4. Type and relative abundance of iron species on S-nZVI surfaces as a function of aging in anoxic artificial groundwater as obtained from curve fitting of high resolution XPS Fe $2p_{3/2}$ spectra according to procedures by Biesinger et al.[5] Specifically, the Fe^0 peak was modelled as an asymmetric line shape (LA (1.1,3.2,3). In addition, Gaussian-Lorentzian peaks were used to model Fe^{2+}-S peak, representing the FeS phase,[8] and five Fe^{2+}-O multiplet peaks representing the Fe (hydr)oxide phase.[5] Note that the peak positions were corrected to adventitious carbon (binding energy, BE = 285 eV).

	day 0		
Species	Peak position, eV (±0.1 eV)	Full width at half-maximum (FWHM), eV	Atomic concentration, %
Fe^0	706.3	0.6	26.52
Fe^{2+}-S	706.6	1.6	25.99
Fe^{2+}-O (1)	708.3	1.4	11.67
Fe^{2+}-O (2)	709.3	1.5	14.47

Fe^{2+}-O (3)	710.5	1.5	7.00
Fe^{2+}-O (4)	711.3	2.6	11.66
Fe^{2+}-O (5)	714.3	2.6	2.68
Fe satellite	716.9	0.3	0.00
		day 10	
Fe^{0}	706.8	0.6	26.74
Fe^{2+}-S	707.1	1.5	24.4
Fe^{2+}-O (1)	708.7	1.9	11.92
Fe^{2+}-O (2)	709.7	1.5	14.77
Fe^{2+}-O (3)	710.8	1.6	7.15
Fe^{2+}-O (4)	711.7	2.5	11.91
Fe^{2+}-O (5)	714.6	2.5	2.74
Fe^{2+} satellite	716.3	2.3	0.39
		day 20	
Fe^{0}	706.7	0.7	26.11
Fe^{2+}-S	707.0	1.6	14.81
Fe^{2+}-O (1)	708.8	1.4	14.03
Fe^{2+}-O (2)	709.9	1.5	17.39
Fe^{2+}-O (3)	711.0	1.5	8.41
Fe^{2+}-O (4)	711.9	2.6	14.02
Fe^{2+}-O (5)	715.1	2.6	3.22
Fe satellite	714.8	3.1	2.01
		day 40	
Fe^{0}	706.9	0.7	19.68
Fe^{2+}-S	707.1	1.6	14.31
Fe^{2+}-O (1)	709.0	1.4	15.87
Fe^{2+}-O (2)	710.2	1.5	19.68
Fe^{2+}-O (3)	711.3	1.6	9.52
Fe^{2+}-O (4)	712.2	2.5	15.86
Fe^{2+}-O (5)	715.2	2.4	3.65
Fe satellite	714.3	1.9	1.43
		day 60	
Fe^{0}	706.7	0.7	15.41
Fe^{2+}-S	707.0	1.7	8.3
Fe^{2+}-O (1)	709.0	1.4	17.86
Fe^{2+}-O (2)	710.1	1.5	22.14
Fe^{2+}-O (3)	711.2	1.6	10.71
Fe^{2+}-O (4)	712.1	2.6	17.85
Fe^{2+}-O (5)	715.0	2.6	4.10
Fe satellite	715.1	2.8	3.63
		day 120	
Fe^{0}	706.6	0.8	7.28
Fe^{2+}-S	706.9	1.8	7.28
Fe^{2+}-O (1)	708.9	1.4	20.30
Fe^{2+}-O (2)	710.1	1.5	25.17

Fe^{2+}-O (3)	711.2	1.5	12.18
Fe^{2+}-O (4)	712.2	2.6	20.29
Fe^{2+}-O (5)	715.1	2.5	4.66
Fe satellite	714.7	2.5	2.84

Table S5. Type and relative abundance of sulfur species on S-nZVI surfaces as a function of aging in anoxic artificial groundwater as obtained from curve fitting of high resolution S 2p spectra following procedures by Mullet et al.[8] Specifically, two multiplet peaks were used to model the sulfur species. The ΔBE, FWHM, and area ratios of the multiplet peaks were fixed.

day 0			
Species	Peak position, eV (±0.1 eV)	Full width at half-maximum (FWHM), eV	Atomic concentration, %
S^{2-} ($2p_{3/2}$)	161.6	1.0	56.83
S^{2-} ($2p_{1/2}$)	162.8	1.0	29.02
S_n^{2-} ($2p_{3/2}$)	163.1	1.0	4.08
S_n^{2-} ($2p_{1/2}$)	164.3	1.0	2.08
S^0 ($2p_{3/2}$)	164.0	1.0	5.29
S^0 ($2p_{1/2}$)	165.2	1.0	2.70
day 10			
S^{2-} ($2p_{3/2}$)	161.8	1.1	49.32
S^{2-} ($2p_{1/2}$)	162.9	1.1	25.19
S_n^{2-} ($2p_{3/2}$)	163.3	1.1	7.97
S_n^{2-} ($2p_{1/2}$)	164.5	1.1	4.07
S0 ($2p_{3/2}$)	165.7	1.1	3.01
S0 ($2p_{1/2}$)	166.9	1.1	1.54
SO_4^{2-} ($2p_{3/2}$)	169.0	1.1	5.89
SO_4^{2-} ($2p_{1/2}$)	170.2	1.1	3.01
day 20			
S^{2-} ($2p_{3/2}$)	162.1	1.1	48.23
S^{2-} ($2p_{1/2}$)	163.2	1.1	24.63
S_n^{2-} ($2p_{3/2}$)	163.6	1.1	7.59
S_n^{2-} ($2p_{1/2}$)	164.8	1.1	3.88
S0 ($2p_{3/2}$)	165.5	1.1	3.10
S0 ($2p_{1/2}$)	166.7	1.1	1.58
SO_4^{2-} ($2p_{3/2}$)	168.9	1.1	7.28
SO_4^{2-} ($2p_{1/2}$)	170.1	1.1	3.72
day 40			

S^{2-} ($2p_{3/2}$)	161.8	1.1	39.37
S^{2-} ($2p_{1/2}$)	162.9	1.1	20.11
S_n^{2-} ($2p_{3/2}$)	163.4	1.1	6.54
S_n^{2-} ($2p_{1/2}$)	164.6	1.1	3.34
S0 ($2p_{3/2}$)	166.2	1.1	3.28
S0 ($2p_{1/2}$)	167.4	1.1	1.67
SO_4^{2-} ($2p_{3/2}$)	168.8	1.1	17.00
SO_4^{2-} ($2p_{1/2}$)	170.0	1.1	8.68
day 60			
S^{2-} ($2p_{3/2}$)	161.6	1.1	32.16
S^{2-} ($2p_{1/2}$)	162.8	1.1	16.43
S_n^{2-} ($2p_{3/2}$)	165.8	1.1	2.29
S_n^{2-} ($2p_{1/2}$)	167.0	1.1	1.17
S0 ($2p_{3/2}$)	163.1	1.1	5.64
S0 ($2p_{1/2}$)	164.3	1.1	2.88
SO_4^{2-} ($2p_{3/2}$)	168.8	1.1	26.10
SO_4^{2-} ($2p_{1/2}$)	170.0	1.1	13.33
day 120			
S^{2-} ($2p_{3/2}$)	161.9	1.2	35.27
S^{2-} ($2p_{1/2}$)	163.1	1.2	18.01
S_n^{2-} ($2p_{3/2}$)	164.3	1.2	4.59
S_n^{2-} ($2p_{1/2}$)	165.5	1.2	2.35
SO_4^{2-} ($2p_{3/2}$)	169.0	1.2	26.33
SO_4^{2-} ($2p_{1/2}$)	170.2	1.2	13.44

Table S6. Relative abundance of total sulfur and total iron species in the top ~10 nm of S-nZVI materials as a function of aging, as determined by wide-XPS measurements. We observed a continuous decrease in sulfur species while iron species increase, with increased aging. This is caused by the enrichment of corrosion products that are larger in volume, thus less S-nZVI are detected.

Aging Time	Sulfur (%)	Iron (%)	S/Fe ratio
0	32.69	67.31	0.49
10	28.23	71.77	0.39
20	24.83	75.17	0.33
40	21.46	78.54	0.27
60	15.81	84.19	0.19
120	10.64	89.36	0.12

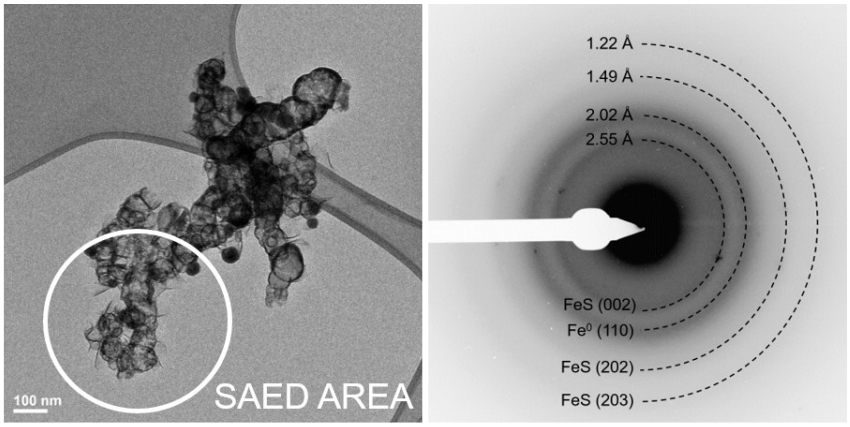

Phase assignment

d-spacing$_{meas}$	Phase	hkl	d-spacing$_{theo}$
2.55 Å	FeS_m	002	2.52 Å
2.02 Å	Fe^0	110	2.03 Å
1.49 Å	FeS_m	202	1.48 Å
1.22 Å	FeS_m	203	1.19 Å

Figure S7. Selected electron area diffraction (SAED) of Figure 4a showing the diffuse rings of Fe^0 and FeS_m, corroborating that no other Fe sulfide phases formed apart from FeS_m.

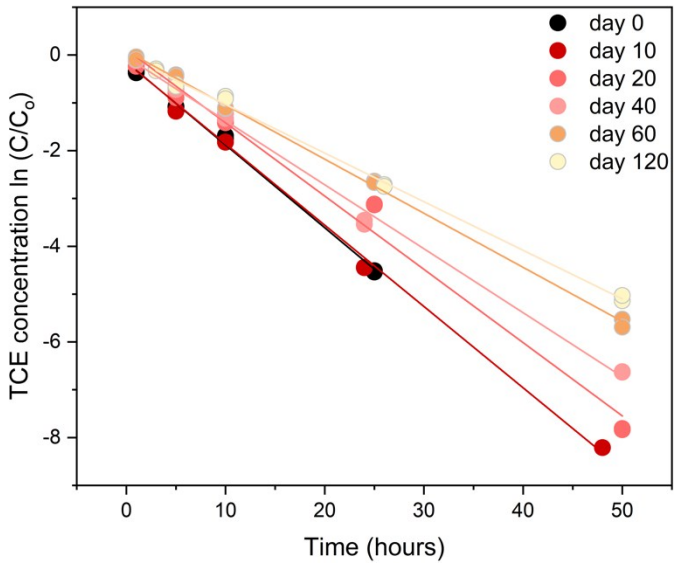

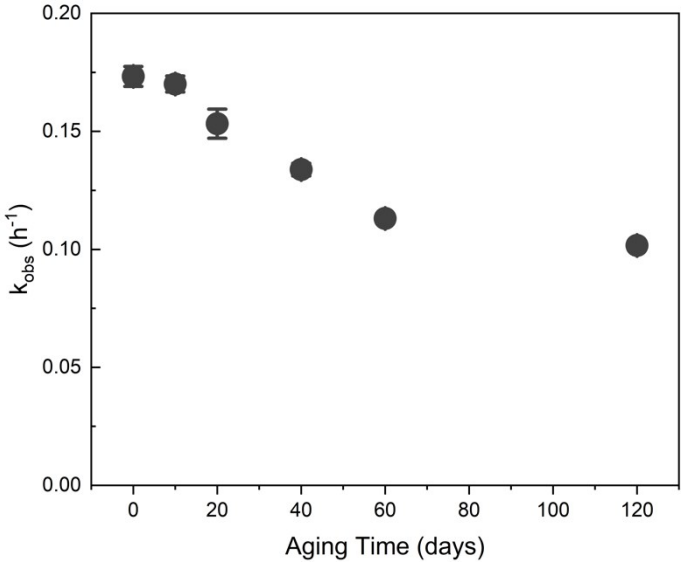

Figure S8. Decrease in normalised TCE concentration over time (top) and calculated k_{obs} (bottom) for progressively aged S-nZVI materials. The plotted TCE concentrations are from duplicate measurements, with the error bars giving the standard error of the fitted k_{obs} (Equation 1). It is evident that despite aging for up to 120 days, all TCE was reduced within 50 h of reaction. This is a clear indication that S-nZVI is able to sustain its reactivity over long time periods.

Table S7. Calculated TCE reduction rate constants (k_{obs}) and its standard error (SE) for S-nZVI materials aged for different time periods.

Aging Time	**Day 0**	**Day 10**	**Day 20**	**Day 40**	**Day 60**	**Day 120**
k_{obs} (h^{-1}) ±	0.173 ±	0.170 ±	0.153 ±	0.134 ±	0.113 ±	0.102 ±
SE	0.004	0.003	0.006	0.003	0.001	0.002

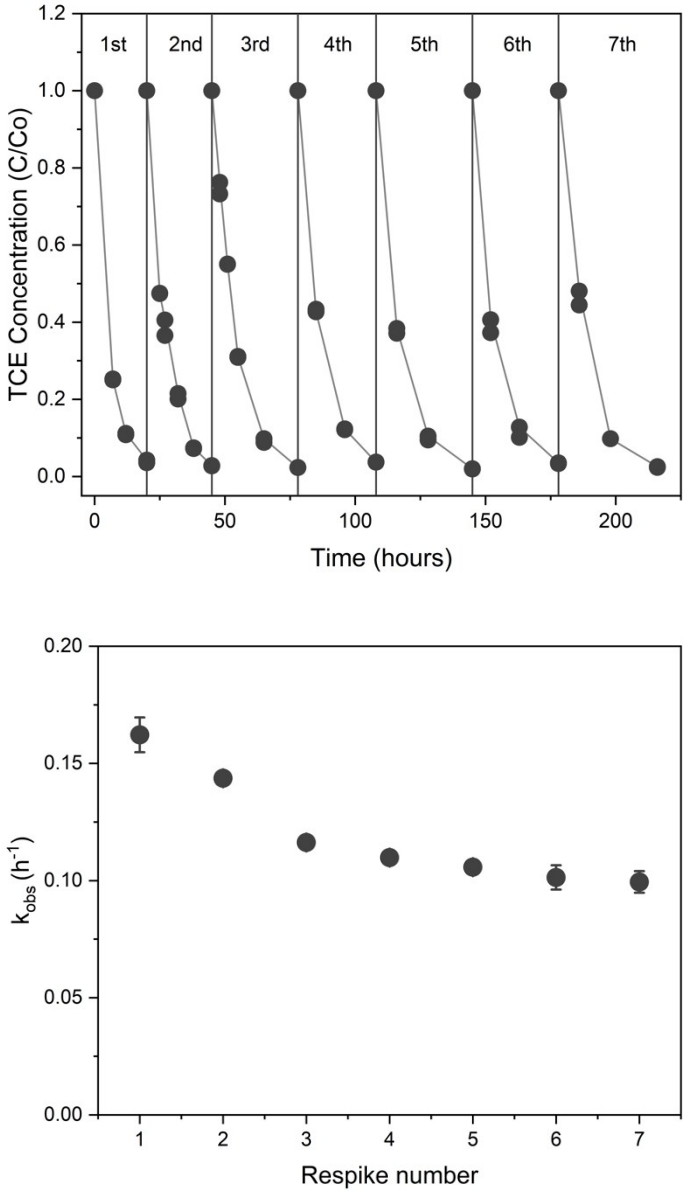

Figure S9. (Top) Plot of TCE re-spiking experiments shows that TCE is consistently reduced by S-nZVI even after 7 TCE amendments. The plotted TCE values are obtained from duplicate measurements. (Bottom) Calculated k_{obs} as a function of TCE re-spike number, with error bars representing the standard error from the linear regression fitting. Assuming that 110 µM of TCE will require 660 µM of electrons (equivalent to 1 re-spike), then the total electrons needed to reduce 770 µM TCE is 4.6 mM. This is equivalent to 25% of the total electron pool available in S-nZVI (assuming that 1 mM of Fe^0 can donate a total of 2 mM e^-).

Table S8. Calculated TCE reduction rate constants (k_{obs}) and its standard error (SE) in TCE re-spiking experiments.

Re-spike cycle	1	2	3	4	5	6	7
k_{obs} (h^{-1})	0.162	0.144	0.116	0.110	0.106	0.101	0.099
±SE	±0.007	±0.003	±0.002	±0.002	±0.003	±0.005	±0.005

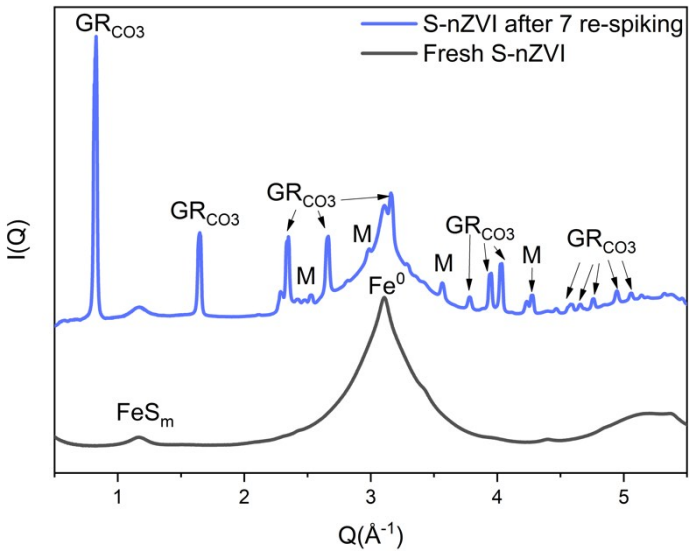

Figure S10. Synchrotron-based XRD pattern of the S-nZVI at the end of TCE re-spiking experiment. Green rust carbonate (GR_{CO3}) is the main oxidation products of the material. Very small peaks of magnetite (M) are also observed, which may stem from the continuous redox process of S-nZVI and TCE. Notably, after 7 re-spikes, the FeS_m peak is still evident and no other FeS phases (i.e., Fe_3S_4, FeS_2) were observed.

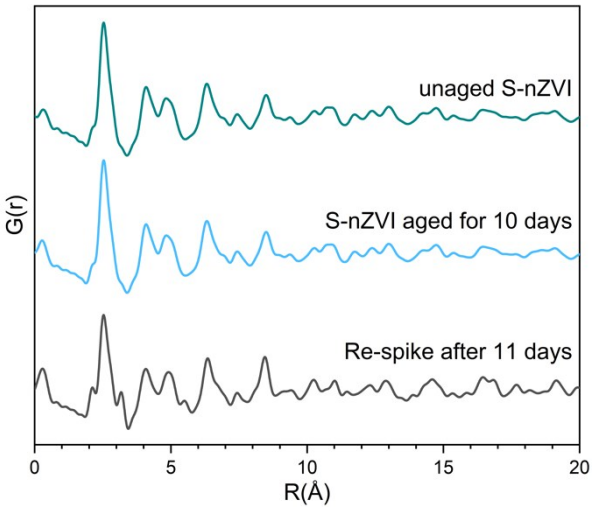

Figure S11. PDF of S-nZVI aged in TCE re-spiking experiment for 11 days (total of 7 re-spikes) exhibits a 21% decrease in Fe^0 peak intensity (at 2.53 Å) relative to the unaged sample. In addition, comparison of PDFs between the re-spiked sample and the 10-day groundwater aged sample (without TCE) shows that the TCE has extensively oxidized the S-nZVI core, relative to water.

References:

(1) Mangayayam, M.; Dideriksen, K.; Ceccato, M.; Tobler, D. J. The Structure of Sulfidized Zero Valent Iron by One-Pot Synthesis: Impact on Contaminant Selectivity and Long-Term Performance. *Environ. Sci. Technol.* **2019**, acs.est.8b06480.

(2) Smith, E. J.; Davison, W.; Hamilton-Taylor, J. Methods for Preparing Synthetic Freshwaters. *Water Res.* **2002**, *36* (5), 1286–1296.

(3) Wyckoff, R. W. *Crystal Structures Vol 1*; Interscience Publishers, New York, 1948.

(4) Christiansen, B. C.; Dideriksen, K.; Katz, A.; Nedel, S.; Bovet, N.; Sørensen, H. O.; Frandsen, C.; Gundlach, C.; Andersson, M. P.; Stipp, S. L. S. Incorporation of Monovalent Cations in Sulfate Green Rust. *Inorg. Chem.* **2014**, *53* (17), 8887–8894.

(5) Biesinger, M. C.; Payne, B. P.; Grosvenor, A. P.; Lau, L. W. M.; Gerson, A. R.; Smart, R. S. C. Resolving Surface Chemical States in XPS Analysis of First Row Transition Metals, Oxides and Hydroxides: Cr, Mn, Fe, Co and Ni. *Appl. Surf. Sci.* **2011**, *257* (7), 2717–2730.

(6) Mullet, M.; Boursiquot, S.; Abdelmoula, M.; Génin, J. M.; Ehrhardt, J. J. Surface Chemistry and Structural Properties of Mackinawite Prepared by Reaction of Sulfide Ions with Metallic Iron. *Geochim. Cosmochim. Acta* **2002**, *66* (5), 829–836.

(7) Mangayayam, M. C.; Dideriksen, K.; Tobler, D. J. Can or Cannot Green Rust Reduce Chlorinated Ethenes? *Energy Procedia* **2018**, *146*, 173–178.

(8) Boursiquot, S.; Mullet, M.; Abdelmoula, M.; Génin, J.-M.; Ehrhardt, J.-J. The Dry Oxidation of

Tetragonal FeS1- x Mackinawite. *Phys. Chem. Miner.* **2001**, *28* (9), 600–611.

(9) The Oxidation of Fe(OH)2 in the Presence of Carbonate Ions: Structure of Carbonate Green Rust One. *Hyperfine Interact.* **1994**, *90* (1), 395–400.